

ForestSplats: Deformable transient field for Gaussian Splatting in the Wild

Wongi Park^{1*}, Myeongseok Nam^{1*}, Siwon Kim¹, Sangwoo Jo² and Soomok Lee^{1†}

¹Ajou University ²Minds and Company
 {psboys, soomoklee}@ajou.ac.kr

<https://forestsplats.github.io/>

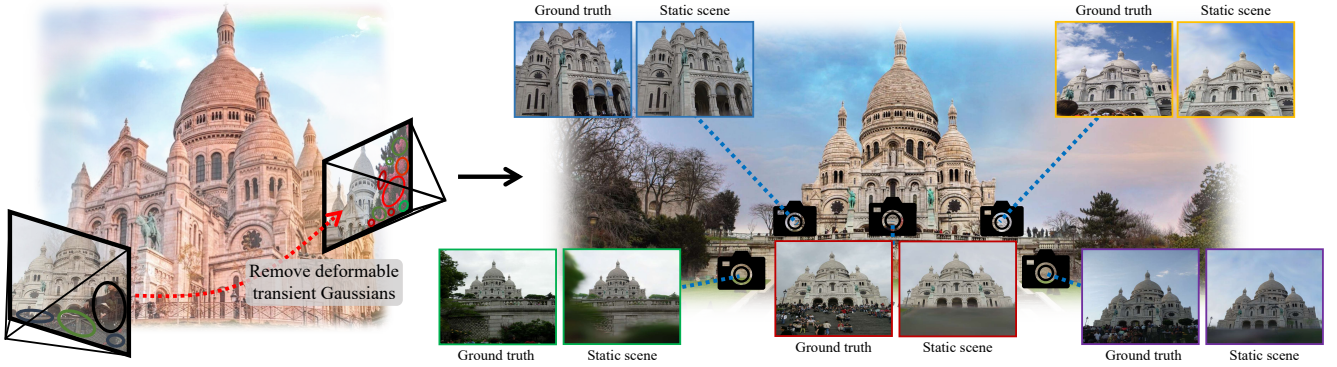


Figure 1. Given unconstrained images, ForestSplats efficiently represents transient elements from 2D scenes and achieves fast rendering speed while preserving high-quality. Our method decomposes the scene into the deformable transient field and the static field to disentangle static and transient elements without a Vision Foundation Model (VFM). More details are available in the supplementary materials.

Abstract

Recently, 3D Gaussian Splatting (3D-GS) has emerged, showing real-time rendering speeds and high-quality results in static scenes. Although 3D-GS shows effectiveness in static scenes, their performance significantly degrades in real-world environments due to transient objects, lighting variations, and diverse levels of occlusion. To tackle this, existing methods estimate occluders or transient elements by leveraging pre-trained models or integrating additional transient field pipelines. However, these methods still suffer from two defects: **1)** Using semantic features from the Vision Foundation model (VFM) causes additional computational costs due to pre-training on external data to use prior knowledge. **2)** The transient field requires significant memory to handle transient elements with per-view Gaussians and struggles to define clear boundaries for occluders, solely relying on photometric errors. To address these problems, we propose **ForestSplats**, a novel approach that leverages the deformable transient field and a superpixel-aware mask to efficiently represent transient elements in the 2D scene across unconstrained image collections and effectively decompose static scenes from transient distrac-

tors without VFM. We designed the transient field to be deformable, capturing per-view transient elements. Furthermore, we introduce a superpixel-aware mask that clearly defines the boundaries of occluders by considering photometric errors and superpixels. Additionally, we propose uncertainty-aware densification to avoid generating Gaussians within the boundaries of occluders during densification. Through extensive experiments across several benchmark datasets, we demonstrate that ForestSplats outperforms existing methods without VFM and shows significant memory efficiency in representing transient elements.

1. Introduction

Novel view synthesis from a sparse set of captured 2D images is a challenging and fundamental problem in computer vision and graphics, which has recently gained popularity. Such advancements play a critical role in applications such as augmented/virtual reality (VR) [5, 6], autonomous driving [12, 47], and 3D content generation [15, 36]. Even though Neural Radiance Field (NeRF) [18] has shown impressive results and rendering efficiency, it suffers from slow rendering speeds. Due to this issue, 3D Gaussian Splatting (3D-GS) [7] recently has emerged as

*Equal contribution.

†Corresponding author.

an explicit 3D representation that offers real-time rendering speeds. However, existing methods [31, 35] assume that 2D images are captured without transient elements, various levels of occluders, or appearance variations such as changing sky, weather, and illumination. Therefore, accurately and robustly reconstructing with unconstrained image collections remains a primary challenge due to many transient elements in real-world environments. Several works have proposed various solutions to tackle this challenge. Early NeRF-based methods [2, 17, 38] introduce per-image transient embedding or photometric errors to typically ignore transient elements from unconstrained images. NeRF-W [17] optimizes an uncertainty embedding to address distractors. CR-NeRF [40] proposes a cross-ray paradigm and grid sampling strategy for efficient appearance modeling. Although showing promising results, these methods [2, 17, 40] are computationally intensive and struggle with real-time rendering. In contrast, 3D-GS-based methods [10, 14, 24, 33, 37] usually utilize semantic features from Vision Foundation Model (VFM) to estimate precise distractors mask, showing fast rendering speed. Wild-GS [37] uses depth information from Depth Anything [39] and a hierarchical decomposition strategy to regularize transient elements and preserve geometry consistency. WildGaussians [10] also utilizes semantic features from DINOv2 [20] to handle occlusions. HybridGS [14] defines a transient field to explicitly decompose transient elements. Despite significant advancements, these methods still suffer from two limitations: **Firstly**, leveraging semantic features from the Vision Foundation Model (VFM) causes additional computational costs due to pre-computation on external huge data to use prior knowledge. **Secondly**, the transient field uses significant memory to handle transient elements using Gaussians per image and struggles to clearly estimate boundaries of occluders due to solely relying on the photometric errors. Our motivation stems from the lack of appearance variation and multi-view consistency in transient elements. That is, we only need to consider transient elements in the 2D scene from each view of unconstrained image scenarios. To end, we propose ForestSplats, which leverages a deformable transient field and superpixel-aware mask to effectively decouple transient elements from static scenes, showing high-quality rendering. We design deformable transient field that efficiently represents transient elements in the 2D scene across unconstrained image collections, which are explicitly decomposed from static field and show memory efficiency. Furthermore, we introduce superpixel-aware masking, which effectively separates distractors from static scenes without a pre-trained VFM by considering the photometric errors and superpixels in the 2D scene. Additionally, we incorporate a multi-stage training scheme to enhance the superpixel-aware mask in accurately capturing transient elements, achieving distractor-free novel-view synthesis. Fur-

thermore, we introduce uncertainty-aware densification for static field, thereby avoiding generating Gaussians within the boundaries of occluders, showing high-quality rendering. Through extensive experiments on several datasets, we demonstrate that ForestSplats effectively decomposes transient elements from static scenes, outperforming the state-of-the-art methods without VFM in novel view synthesis. Our primary contributions can be summarized as follows.

- We propose ForestSplats, which explicitly decomposes 3D scenes into static and deformable transient fields, effectively capturing static scenes while demonstrating memory efficiency to represent transient elements.
- We introduce a superpixel-aware mask and a multi-stage training scheme that effectively separate the 3D scene representation into static and transient fields by considering the photometric errors and the superpixels.
- We introduce uncertainty-aware densification to avoid generating Gaussians within the boundaries of occluders.
- Extensive experiments demonstrate that ForestSplats achieves state-of-the-art performance and shows memory efficiency to represent transient elements.

2. Related Works

3D Scene Decomposition. Early decomposition-based approaches [19, 21, 38] have been widely used in dynamic 3D novel view synthesis, decoupling dynamic objects from static scenes by comparing successive video frames and identifying differences as foreground elements. These methods [19, 21, 29, 38] achieve more effective partitioning of static and dynamic elements by modeling scene dynamics through deformations of a canonical volume, particle-level motion, or rigid transformations of local geometric primitives. Meanwhile, another line of work [11, 14, 17, 33] focuses on static scenes by disentangling transient objects and lighting variations while utilizing per-view transient Gaussians or a transient field. However, these approaches [14, 33] assign each Gaussian primitive to an individual image, increasing the number of transient Gaussian primitives, which requires inefficient memory usage. In contrast, we introduce a deformable transient field, enabling the efficient representation of transient elements across unconstrained image collections, showing high-quality rendering without excessive memory consumption.

Uncertainty in 3D Scene Reconstruction. Recent novel view synthesis methods [7, 18, 26] rely on the assumption of distractor-free environments. However, unconstrained image collections often violate these assumptions due to dynamic elements, lighting variations, and other transient factors. Numerous earlier methods [11, 17, 18, 40] utilize implicit neural representation to encode 3D scenes, with differentiable volume rendering along the rays. NeRF-W [17] optimizes a transient field and an uncertainty embedding

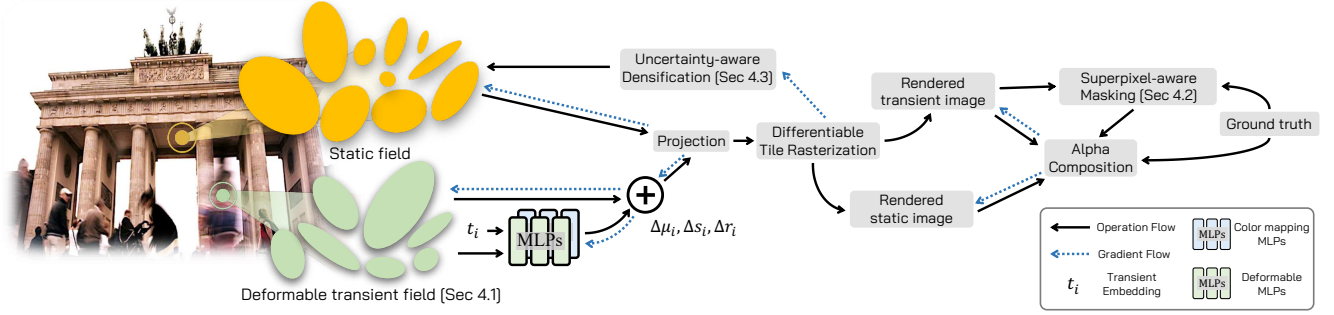


Figure 2. An overview of ForestSplats. We decompose the 3D scene into the static and deformable transient fields. The rendered images combine alpha blending with a mask to produce compositional rendering results. Furthermore, we leverage a superpixel-aware mask, which considers photometric errors and superpixels to effectively decompose static and transient elements. Specifically, during optimization, we leverage uncertainty-aware densification (UAD) to avoid generating static Gaussians within the boundaries of occluders.

per view to address distractors. CR-NeRF [40] introduces a cross-ray paradigm and a grid sampling strategy for efficient appearance modeling. NeRF-MS [11] tackles multi-sequence images captured in the wild using triplet loss and a decomposition module with several transient embeddings. While NeRF-based methods [11, 17, 18, 40] offer efficient and high-quality 3D rendering, they are still computationally resource-intensive and limit real-time rendering speed. On the other hand, 3D-GS-based methods [7, 10, 37, 39] explicitly represent the 3D scene with differentiable rasterization, showing fast rendering speed and high-quality results. Wild-GS [37] leverages depth information from pre-trained Depth Anything [39] and a hierarchical decomposition strategy to regularize transient elements and preserve geometry consistency. WildGaussians [10] also utilizes semantic features of pre-trained DINOv2 [20] to handle transient elements. Unlike these approaches, our method effectively decomposes distractors from static scenes and represents transient elements without pre-trained VFM by leveraging photometric errors and superpixels.

Adaptive Density Control of 3D Gaussians. Adaptive density control (ADC) strategy in 3D Gaussian Splatting works [7] through two operations, densification and pruning, which capture empty areas or fine details during optimization. While showing efficiency, this ADC module relies on predetermined thresholds and does not leverage context information, leading to blurriness in high-frequency details in sparse point areas. To tackle this, Pixel-GS [46] leverages the number of pixels covered by Gaussian primitives as weights to promote densification, complementing average 2D position gradients. Taming-3DGS [16] proposes score-based densification and steerable densification strategies, ordered by high opacity, improving the quality per Gaussian while avoiding an overemphasis on specific regions during training. Unfortunately, most existing methods [7, 16, 46] improve rendering quality in constrained image collections, but their application to unconstrained image

collections is limited and remains challenging due to transient elements. In this work, we aim to develop an efficient densification strategy for casually captured images in the wild. To this end, we assign learnable uncertainty attributes to each Gaussian, removing high-uncertainty Gaussians in the static field. Furthermore, we effectively refine densification to avoid generating Gaussians within the boundaries of occluders during densification by considering positional gradient and the number of pixels covered by Gaussians.

3. Preliminary

3D Gaussian Splatting (3D-GS). 3D Gaussian Splatting (3D-GS) [7] has emerged as a promising method for novel view synthesis, representing a scene as a set of differentiable Gaussians $\{\mathcal{G}_i\}$. Each Gaussian \mathcal{G}_i is parameterized by a position $\mu_i \in \mathbb{R}^3$, covariance matrix $\Sigma_i \in \mathbb{R}^{3 \times 3}$, which is decomposed into rotation matrix $R \in \text{SO}(3)$, and scaling matrix $S \in \mathbb{R}^{3 \times 3}$, an opacity $\alpha_i \in [0, 1]$, and view-dependent colors $c_i \in \mathcal{C}^{N_{sh}}$ represented via spherical harmonics (SH) coefficients N_{sh} . To render images, 3D Gaussians $\{\mathcal{G}_i\}$ are projected onto screen space as 2D Gaussians via the viewing transformation $W \in \mathbb{R}^{3 \times 3}$ and covariance matrix $\Sigma'_i = JW\Sigma_iW^TJ^T$ where $J \in \mathbb{R}^{2 \times 3}$ is the Jacobian of the Taylor approximation of the projective transformation. For each pixel, the K Gaussians $\{\mathcal{G}_k \mid k = 1, \dots, K\}$ are ordered by depth and rendered using alpha-blending, resulting in pixel color \hat{C} :

$$\hat{C} = \sum_{k=1}^K c_k \alpha_k \prod_{j=1}^{k-1} (1 - \alpha_j). \quad (1)$$

All attributes of Gaussian $\{\mathcal{G}_i\}$ are optimized by minimizing the following reconstruction loss between rendered image $\hat{I} \in \mathbb{R}^{3 \times H \times W}$ and ground truth image $I_{gt} \in \mathbb{R}^{3 \times H \times W}$.

$$\mathcal{L}_{GS} = (1 - \lambda)\mathcal{L}_1(\hat{I}, I_{gt}) + \lambda\mathcal{L}_{D-SSIM}(\hat{I}, I_{gt}), \quad (2)$$

where \mathcal{L}_1 is an L_1 loss, \mathcal{L}_{D-SSIM} is a SSIM loss and λ is a weighting factor. All 3D Gaussians are initialized using a sparse point cloud obtained from the Structure-from-

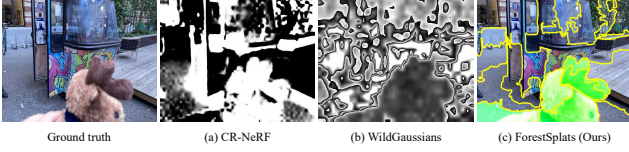


Figure 3. Comparison of transient masking methods. (a) CR-NeRF focuses only on the photometric errors, (b) WildGaussians considers the semantic features, and (c) ForestSplats leverages photometric errors and superpixels to capture transient elements.

Motion (SfM) approach such as COLMAP [25]. Meanwhile, to effectively control the density of Gaussians and address under and over-reconstruction problems, adaptive densification and pruning strategies are employed to enhance the 3D scene reconstruction during optimization.

4. Method

Given unconstrained image collections, our goal is to represent the static scene and effectively remove all transient elements in 2D scenes. To this end, we propose ForestSplats, which leverages a deformable transient field and a superpixel-aware mask to effectively separate static scenes from transient distractors in 2D scenes. Firstly, we describe a deformable transient field to represent transient elements across unconstrained image collections without excessive memory usage in Sec. 4.1. Then, in Sec. 4.2, we propose a superpixel-aware mask to clearly separate a static scene from diverse occluders in 2D scenes. Finally, we introduce uncertainty-aware densification to avoid generating Gaussians within the boundaries of occluders, as described in Sec. 4.3. The overview of our method is depicted in Fig. 2.

4.1. Deformable Transient Field

Our primary objective is to decompose a 3D scene into transient and static fields while effectively identifying distractors. Although existing methods [11, 14, 17, 33] utilize stationary transient field or per-view Gaussians to represent transient elements, prior methods are either limited in effectively capturing transient elements per image or show excessive memory usage, as shown in Tab. 3. To mitigate these limitations, we propose a deformable transient field \mathcal{G}_d to efficiently represent transient elements per image across unconstrained photo collections. We follow the paradigm of Deform3D-GS [41] to represent transient elements for each view I_{gt} . Our method represents each view \hat{I} as the sum of transients $\hat{I}_d \in \mathbb{R}^{3 \times H \times W}$ and statics $\hat{I}_s \in \mathbb{R}^{3 \times H \times W}$ through a mask $M \in [0, 1]$ such that:

$$\hat{I} = M \odot \hat{I}_d + (1 - M) \odot \hat{I}_s. \quad (3)$$

Given transient embedding per image t_i and position μ_i of transient 3D Gaussians $\mathcal{G}_d(\mu_i, s_i, r_i)$ as inputs, the deformation transient MLP f_d predicts transient elements, producing the offset $\Delta\mu$, Δs , and Δr . Furthermore, transient

elements in unconstrained images have inconsistent colors across views. Therefore, we additionally introduce the transient color MLP f_c to map the color of transient elements expressed as:

$$(\Delta\mu, \Delta s, \Delta r) = f_d(\gamma(\text{sg}(\mu)), \gamma(t)), \quad \hat{c} = f_c(\gamma(t)), \quad (4)$$

where $\text{sg}(\cdot)$ is the stop-gradient operation, and $\gamma(\cdot)$ denotes the positional encoding. Finally, the transient 3D gaussians is computed as $\mathcal{G}_d(\mu_i + \Delta\mu_i, s_i + \Delta s_i, r_i + \Delta r_i)$ to represent transient elements. Our method differs from Deform3D-GS [41] in one important way: instead of representing dynamic elements that are successively consistent in each image, our primary goal is to efficiently capture ephemeral and transient elements by leveraging deformable transient field showing significant memory efficiency.

4.2. Superpixel-aware Mask

Existing methods [10, 23, 24, 44] primarily address outlier handling using Least Squares techniques or by extracting semantic features from the Vision Foundation Model (VFM). Inspired by these works, we propose a superpixel-aware mask and a multi-stage training scheme that effectively decompose transient distractors from static scenes. Our approach considers photometric errors and superpixels. Following CR-NeRF [40], we obtain the transient mask \mathcal{M}_O from Unet S_θ through a learning-based approach, optimizing to minimize the training loss without per-scene optimization. However, directly using the transient mask \mathcal{M}_O often struggles with imprecise boundaries of occluders, as shown in Fig. 3. To tackle this, we leverage the superpixel algorithm [30], which considers color and spatial information. Given an each view I_{gt} partitioned into set of superpixels $\mathcal{S} = \{s_1, \dots, s_j\}$, we compute the mask coverage ratio ρ_j for each superpixel s_j as follow:

$$\rho_j = \frac{|\{p \in s_j \mid \mathcal{M}_{O^*}(p) = 1\}|}{|s_j|}, \quad \mathcal{M}_{O^*} = \mathcal{M}_O > 0.5, \quad (5)$$

where p is pixel position. We employ a threshold to prevent Gaussians from being ambiguously assigned between the static and transient fields. Consequently, the superpixel-aware mask \mathcal{M}_S is defined as:

$$\mathcal{M}_S(p) = \begin{cases} \max_{p \in s_j} \mathcal{M}_{O^*}(p), & \text{if } \rho_j \geq 0.5 \text{ for } p \in s_j \\ \mathcal{M}_{O^*}(p), & \text{otherwise} \end{cases} \quad (6)$$

Additionally, to prevent \mathcal{M}_O from masking everything, we add a regularization term following CR-NeRF [40]. Furthermore, to mitigate the undesired blending of Gaussians between static and transient fields, we introduce the loss term $\mathcal{L}_{BCE}(\mathcal{M}_O, \mathcal{M}_S)$. Finally, the total loss function is defined as follows:

$$\mathcal{L}_{\text{total}} = (1 - \lambda) \mathcal{L}_1(\hat{I}, I_{gt}) + \lambda \mathcal{L}_{\text{D-SSIM}}(\hat{I}, I_{gt}) + \lambda_0 \mathcal{L}_{BCE}(\mathcal{M}_O, \mathcal{M}_S) + \lambda_1 \|\mathcal{M}_O\|^2, \quad (7)$$

where λ_0 is $3e - 2$, and λ_1 is $5e - 4$. We observe that initially incorporating the transient mask during training leads



Figure 4. Qualitative results from novel-view synthesis on the Photo Tourism dataset. ForestSplats demonstrates geometry consistency and captures fine details compared to existing methods. Yellow and green crop emphasize appearance differences and consistency differences.

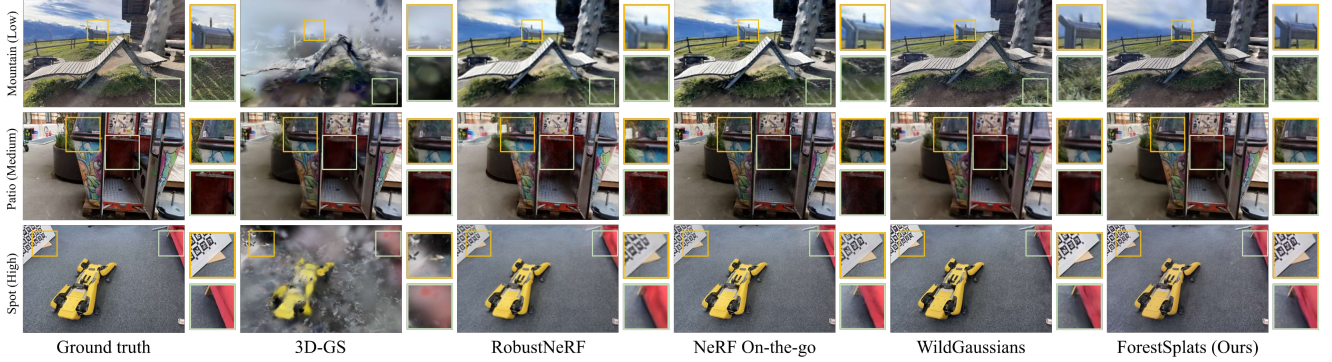


Figure 5. Qualitative results from novel-view synthesis on the NeRF On-the-go dataset. ForestSplats effectively removes distractors and reduces artifacts compared to prior methods. Yellow and green crop primarily emphasize artifacts differences and consistency differences.

to an ambiguous separation between the static and transient fields. To this end, we propose a multi-stage training scheme to resolve the ambiguity between the static and transient fields. Initially, we train the static field to represent the entire image as follows:

$$\mathcal{L}_{\text{init}} = (1 - \lambda)\mathcal{L}_1(\hat{I}_s, I_{gt}) + \lambda\mathcal{L}_{\text{D-SSIM}}(\hat{I}_s, I_{gt}). \quad (8)$$

After enough training time, we train the Unet S_θ and the transient field to capture the transient elements through the following learning process:

$$\mathcal{L}_{\text{mid}} = \mathcal{L}_{\text{total}} + \mathcal{L}_1(\hat{I}_d \odot \bar{\mathcal{M}}_S, I_{gt} \odot \bar{\mathcal{M}}_S), \quad (9)$$

where $\bar{\mathcal{M}}_S$ is calculated as $\bar{\mathcal{M}}_S = 1 - \mathcal{M}_S$. Finally, we jointly train static and transient fields as shown in Eq. 7. This multi-stage training scheme enhances the static field to capture static scenes while achieving high-quality results.

4.3. Uncertainty-aware Densification

During optimization in joint training with densification, we observe that static field \mathcal{G}_s often generates Gaussians near the boundaries of distractors due to random sampling from the probability density function (PDF), as illustrated in Fig. 6-(a). To address this, we propose a simple yet effective uncertainty-aware densification, which introduces un-

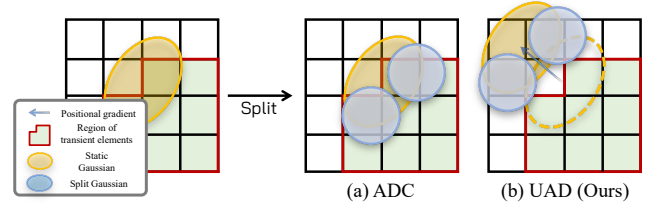


Figure 6. Illustration of ADC and UAD. (a) The existing adaptive density control (ADC) splits Gaussians by sampling from the PDF. In contrast, (b) Uncertainty-aware densification (UAD) splits Gaussians by considering the direction of positional gradients.

certainty parameters $l^{(u)}$ for each static Gaussian and considers the positional gradient and the number of pixels covered by the Gaussian. After the initial training, the uncertainty parameters $l^{(u)}$ are optimized guided by superpixel-aware mask \mathcal{M}_S as follow:

$$\mathcal{L}_t = -\frac{1}{H \times W} \sum_{i=1}^{H \times W} \left[\mathcal{M}_{S,i} \log(\hat{\mathcal{M}}_{l^{(u)},i}) + (1 - \mathcal{M}_{S,i}) \log(1 - \hat{\mathcal{M}}_{l^{(u)},i}) \right], \quad (10)$$

where $\hat{\mathcal{M}}_{l^{(u)}}$ is calculated as $(\sum_{k=1}^K l_k^{(u)}) \odot \mathcal{M}_S$. According to existing methods [4, 46], large Gaussians often cover

Method	GPU hrs / FPS	Low Occlusion			Medium Occlusion			High Occlusion			Average		
		PSNR ↑	SSIM ↑	LPIPS ↓	PSNR ↑	SSIM ↑	LPIPS ↓	PSNR ↑	SSIM ↑	LPIPS ↓	PSNR ↑	SSIM ↑	LPIPS ↓
RobustNeRF [23]	- / <1	16.60	0.407	0.480	21.72	0.741	0.248	20.60	0.602	0.379	19.64	0.583	0.369
Gaussian Opacity Field [43]	0.41 / 43	20.54	0.662	<u>0.178</u>	19.39	0.719	0.231	17.81	0.578	0.430	19.24	0.656	0.280
3D-GS [7]	0.35 / 116	19.68	0.649	0.199	19.19	0.709	0.220	19.03	0.649	0.340	19.30	0.669	0.253
Mip-Splatting [42]	0.18 / 82	20.15	0.661	0.194	19.12	0.719	0.221	18.10	0.664	0.333	19.12	0.681	0.249
GS-W [44]	0.55 / 71	18.67	0.595	0.288	21.50	0.783	0.152	18.52	0.644	0.335	19.56	0.674	0.258
NeRF On-the-go [22]	43 / <1	20.63	0.661	0.191	22.31	0.780	0.130	22.19	0.753	0.169	21.71	0.731	0.163
WildGaussians [10]	0.50 / 108	20.62	0.658	0.235	22.80	0.811	0.092	23.03	0.771	0.172	22.15	0.756	0.167
SpotLessSplats* [24]	0.34 / 93	20.01	0.596	0.276	22.79	0.816	0.161	21.91	0.71	0.222	21.57	0.707	0.219
DeSplat [33]	0.24 / 106	19.93	0.695	0.170	23.47	<u>0.845</u>	<u>0.100</u>	<u>24.33</u>	0.870	0.105	22.58	<u>0.803</u>	0.125
HybridGS [14]	-	<u>21.42</u>	<u>0.684</u>	0.268	<u>23.51</u>	0.830	0.160	23.05	0.768	0.204	<u>22.66</u>	0.761	0.211
ForestSplats (Ours)	1.13 / 117	21.89	0.738	0.216	23.96	0.870	0.135	24.34	<u>0.815</u>	<u>0.119</u>	23.40	0.807	<u>0.156</u>

Table 1. Quantitative result on NeRF On-the-go dataset. The bold and underlined numbers indicate the best and second-best results. Our method shows competitive performance compared to existing methods. More results are reported in the supplementary material.

Method	Photo Tourism			
	GPU hrs / FPS	PSNR ↑	SSIM ↑	LPIPS ↓
3D-GS [7]	2.2 / 57	18.04	0.814	0.183
NeRF-W [17]	164 / <1	20.78	0.799	0.208
Ha-NeRF [18]	452 / <1	21.41	0.793	0.178
DeSplat [33]	-	22.83	0.854	0.182
CR-NeRF [40]	101 / 0.02	23.36	0.812	0.155
RobustNeRF [23]	- / <1	23.44	0.853	0.134
IE-NeRF [32]	- / <1	22.15	0.826	0.181
SWAG [3]	0.8 / 15	23.53	0.868	0.177
WildGaussians [10]	7.2 / 117	24.65	0.851	0.179
NexusSplats [28]	6.81 / -	24.95	0.849	0.185
GS-W [44]	1.2 / 51	24.70	0.865	<u>0.124</u>
Wild-GS [37]	0.52 / 227	26.36	0.873	0.128
ForestSplats (Ours)	7.9 / 122	<u>25.36</u>	<u>0.871</u>	0.151

Table 2. Quantitative average result on the Photo Tourism dataset. The bold and underlined indicate the best and second-best results.

a small area depending on the viewpoint. Inspired by this, we improve the splitting process by shifting static Gaussians along their positional gradient \mathbf{g}_i , weighted by the number of pixels covered by each Gaussian, computed as $\mathbf{g}_i \times (\frac{|\{p|p \in \mathbf{G}_i\}|}{H \times W})$. Subsequently, we apply random sampling from the PDF to avoid splitting the static Gaussians lying in a region of transient elements as shown in Fig. 6-(b). For above the threshold, similar to 3D-GS-based methods, we remove the static Gaussians with high uncertainty to ensure high-quality and consistent rendering results.

5. Experiments

Datasets, metrics, and baseline. Following existing methods [10], we evaluate our method on two datasets: the NeRF On-the-go dataset [22] and the Photo Tourism dataset [27]. The NeRF On-the-go dataset [22] contains twelve scenes, casually captured in indoor and outdoor settings, with three varying levels of occlusion (ranging from 5% to 30%). For a fair comparison, we utilize six scenes and follow the version

*The results are reproduced from the official code.

Scene	Method	Memory	Scene	Method	Memory
Patio high	Desplat [33]	49.96	Corner	Desplat [33]	31.51
	HybridGS [14]	76.22		HybridGS [14]	48.07
	ForestSplats (Ours)	3.28		ForestSplats (Ours)	2.27
Brandenburg Gate	Desplat [33]	304.47	Sacre Coeur	Desplat [33]	260.61
	HybridGS [14]	464.43		HybridGS [14]	397.33
	ForestSplats (Ours)	4.41		ForestSplats (Ours)	3.39

Table 3. Ablation of computational efficiency. We report CPU Memory usage (MB) for initial the number of transient Gaussians.

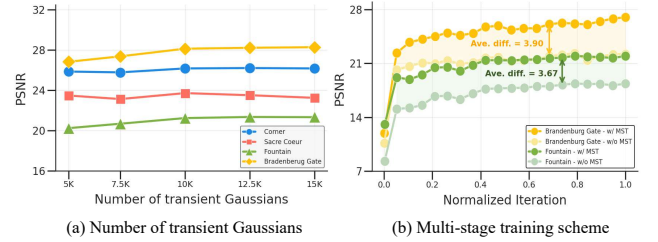


Figure 7. Ablation of the number of transient Gaussians and the multi-stage training scheme. (a) Evaluation of results across different numbers of transient Gaussians. (b) Comparison of training PSNR with and without a multi-stage training scheme.

of the dataset where all images were undistorted as [10]. The Photo Tourism dataset [27] includes several scenes of well-known monuments. Each scene consists of a collection of user-uploaded unconstrained images captured at different dates, times of day, and exposure levels, covering a wide range of lighting conditions. In our experiments, we utilize three scenes: Brandenburg Gate, Sacre Coeur, and Trevi Fountain. We evaluate our method without including occluders in the image, following previous methods [10, 37, 40]. To demonstrate the effectiveness of our method, we use PSNR, SSIM [34], and LPIPS [45] as metrics to evaluate the performance of our proposed method.

Implementation details. We develop our ForestSplats method based on WildGaussians [10]. We follow the hyperparameter settings for the default setting and train using

Scene	Transient Field	PSNR \uparrow	SSIM \uparrow	LPIPS \downarrow
Corner	w/o deformable	24.52	0.855	0.153
	w/ deformable	26.17	0.891	0.136
Brandenburg Gate	w/o deformable	26.83	0.925	0.133
	w/ deformable	28.13	0.935	0.128

Table 4. Ablation of the with and without Deformable for effect of transient field on the Brandenburg Gate and Corner scenes.

the Adam [8] optimizer without weight decay. Specifically, we conducted the improved ADC solely for a static field. Furthermore, we extended the implementation by adapting the Pixel-GS [46] to calculate the number of per-pixel Gaussians using a custom CUDA kernel. For transient elements, we adopt the transient field initialized by randomly selecting 10K points from those obtained through SfM. The deformable MLP consists of eight fully connected layers. In the initial training phase, we conduct 150K steps of training solely on the static field to represent the entire image. Subsequently, we proceed to joint training, where both static and transient fields are optimized until 200K iterations. Finally, we focus on training the static field to capture the static scene. For a fair comparison, we use NerfBaselines [9] as our evaluation framework, providing a unified interface to the originally released source codes. All experiments are performed on an NVIDIA RTX 24GB GPU.

6. Evaluation

Comparison on the Photo Tourism Dataset. As shown in Fig. 4 and Tab. 2, our method shows favorable performance compared to prior methods. In Fig. 4, we observe that CR-NeRF [40], 3D-GS [7], and GS-W [44] frequently fail to capture fine details in scenarios with appearance variations and struggle to handle transient elements. Unlike existing methods, WildGaussians [10] and Wild-GS [37] leverage semantic features from pre-trained VFM [20, 39] to handle the transient elements. In contrast, our ForestSplats effectively decomposes transient elements from 2D scenes by leveraging transient field and a superpixel-aware mask without VFM, demonstrating competitive performance, as shown in Tab. 2. More details are in the supplements.

Comparison on the NeRF On-the-go Dataset. Furthermore, we also show the results for the NeRF On-the-go dataset [22]. Our method also achieves competitive performance against existing SOTA methods across various occlusion levels while enabling real-time rendering without VFM in Tab. 1. Compared to RobustNeRF [23], and NeRF On-the-go [22], our method exhibits faster training and rendering speeds while mitigating negative occluders. RobustNeRF [23] considers photometric errors and the small size of the sampled patches to overlook complex structures and

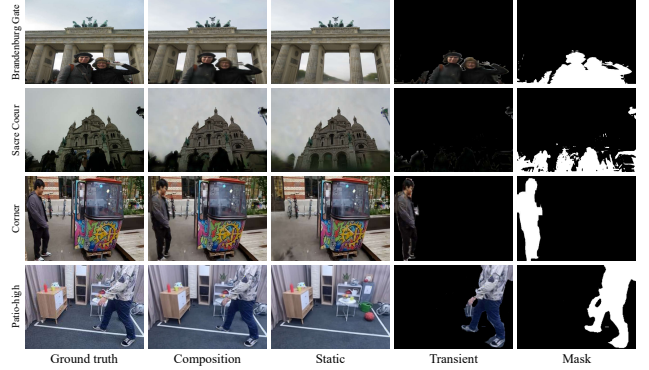


Figure 8. Ablation of the novel-view synthesis for static and transient fields on the NeRF On-the-go and Photo Tourism datasets.

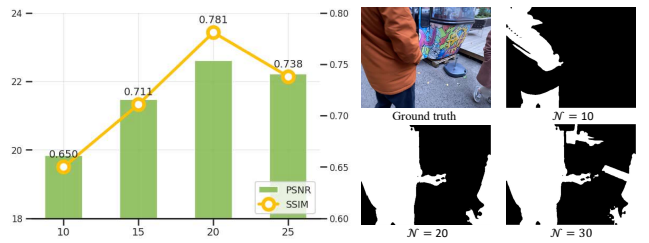


Figure 9. Ablation of the number of superpixels on the Patio-high scene. \mathcal{N} denotes the number of superpixels.

high occlusion scenarios. Specifically, WildGaussians [10] and SpotLessSplats [24] effectively remove transient elements by considering semantic features. Although leveraging semantic features facilitates handling transient elements, distinguishing semantic features similar to static elements remains challenging. However, our method explicitly decomposes static and transient elements across different levels of occluder scenarios, as shown in Fig. 5. Furthermore, compared to the prior methods without VFM, our method outperforms average performance in terms of PSNR and SSIM. We provide more results in the supplements.

7. Ablation Study

Efficiency of Deformable Transient Field. As shown in Tab. 3, the deformable transient field significantly reduces the CPU memory usage (MB). Specifically in the Sacre Coeur, although transient embedding per image is considered, the deformable transient field achieves over an 80% improvement in CPU memory efficiency (MB). Compared to existing methods [14, 33], the deformable transient field enables all transient Gaussians to be loaded onto the GPU, avoiding unnecessary context switching between the CPU and GPU. Furthermore, we also analyze the performance based on the number of transient Gaussians as shown in Fig. 7-(a). We observe that the number of transient Gaussians primarily aims to occupy the regions with transient el-

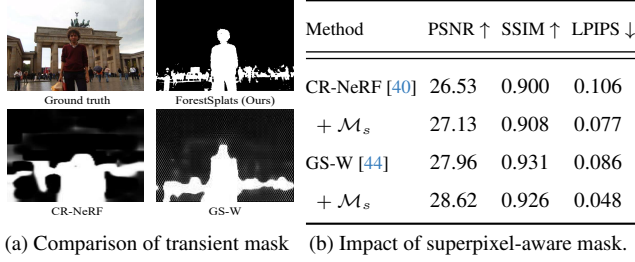


Figure 10. Ablation of the transient mask. (a) Comparison of transient mask methods. (b) Effect of the superpixel-aware mask.

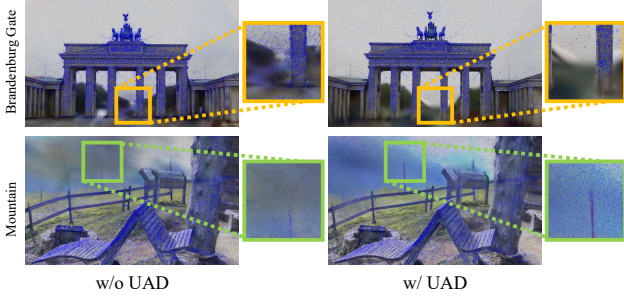


Figure 11. Ablation of the uncertainty-aware densification (UAD). We visualize centroids of static Gaussians with and without UAD.

ements, which results in a slight effect on the representation of the static field. Moreover, we compare the transient field with and without the deformation MLP, as shown in Tab. 4. These results indicate that the deformable transient field not only significantly reduces memory usage (MB) but also facilitates scalability, particularly in large-scale scenarios.

Effectiveness of superpixel-aware mask. We conducted an ablation study to assess the effectiveness of a superpixel-aware mask in handling transient elements. As shown in Fig. 8, our method explicitly decomposes distractors from the static scene and represents transient objects in various scenarios, handling varying levels of occlusion. Furthermore, we analyze the effect of the number of superpixels in Fig. 9. According to the results, a small number of superpixels has minimal effect on the transient mask. Meanwhile, a large number of superpixels may lead to excessive masking of irrelevant areas. Thus, we set the number of segments to 20 as an optimal number. Moreover, we compare the quality of the transient mask in Fig. 10-(a). Existing methods [40, 44] rely on photometric errors. In contrast, superpixel-aware masks leverage superpixels, which consider both color and spatial information, to enhance mask quality without additional memory cost. Furthermore, the superpixel-aware mask serves as a plug-and-play module that combines with existing transient mask methods, showing improved performance, as shown in Fig. 10-(b). The results indicate that the superpixel-aware mask improves performance, achieving an average of 1.47 dB in PSNR and 0.022 in SSIM. Furthermore, we demonstrate a multi-stage



Figure 12. Ablation study of the qualitative results for each component in ForestSplats. More details are provided in the supplements.

Methods	PSNR \uparrow	SSIM \uparrow	LPIPS \downarrow
Baselines [33]	20.14	0.868	0.178
+ Deformable transient Field	22.38	0.861	0.175
+ Superpixel-aware Mask	22.75	0.869	0.162
+ Multi-stage training scheme	23.20	0.861	0.131
+ Uncertainty-aware Densification	23.31	0.867	0.146
+ Pixel-aware gradient (Full)	23.84	0.876	0.123

Table 5. Ablation of the effectiveness of each component in ForestSplats. We report all quantitative results on the Sacre Coeur scene.

training scheme that consistently improves performance in Fig. 7-(b). More results are provided in the supplements.

Discussion on uncertainty-aware densification. We use uncertainty-aware densification (UAD) only in the static field to avoid the generation of static Gaussians at the boundaries of distractors during optimization. To analyze this, we investigate an ablation study with and without UAD to see its effect on novel-view synthesis. As shown in Fig. 11, we observe that the centroids of static Gaussians are primarily positioned on static elements, mitigating the artifacts in novel view synthesis.

Analysis of each component. For further analysis, we evaluate each component of our method to demonstrate the effectiveness: Deformable transient field (DTF), Superpixel-aware mask (SAM), Multi-stage training scheme (MST), and Uncertainty-aware densification (UAD) as shown in Tab. 5. The results indicate that a superpixel-aware mask, which considers the photometric errors and the superpixels, combined with a multi-stage training scheme, consistently improves performance by effectively removing transient elements in scenes. Furthermore, we show qualitative results on the Brandenburg Gate and Corner scenes in Fig. 12.

8. Limitation and Conclusion

Limitation. Although the transient field does not exhibit high quality due to deformable Gaussians, as shown in Fig. 8, the deformable transient field effectively captures transient elements while showing significant memory efficiency. Another limitation of our forestsplats is its difficulty in generalizing the number of superpixels due to the varying levels of occlusion in datasets, as depicted in Fig. 9.

Conclusion. In this paper, we introduce ForestSplats, a novel framework that leverages a deformable transient field

and a superpixel-aware mask to effectively remove distractors from static scenes. Furthermore, we propose a simple yet effective uncertainty-aware densification to enhance rendering quality and avoid generating static Gaussians on the boundaries of distractors during optimization. Extensive experiments on several datasets demonstrate that our method shows state-of-the-art performance compared to existing methods without a pre-trained model and shows significant memory efficiency to represent transient elements.

References

- [1] Holger Caesar, Varun Bankiti, Alex H Lang, Sourabh Vora, Venice Erin Liong, Qiang Xu, Anush Krishnan, Yu Pan, Giancarlo Baldan, and Oscar Beijbom. nuscenes: A multi-modal dataset for autonomous driving. In *Proceedings of the IEEE/CVF conference on computer vision and pattern recognition*, pages 11621–11631, 2020. 13
- [2] Xingyu Chen, Qi Zhang, Xiaoyu Li, Yue Chen, Ying Feng, Xuan Wang, and Jue Wang. Hallucinated neural radiance fields in the wild. In *Proceedings of the IEEE/CVF Conference on Computer Vision and Pattern Recognition*, pages 12943–12952, 2022. 2
- [3] Hiba Dahmani, Moussab Bennehar, Nathan Piasco, Luis Roldao, and Dzmitry Tsishkou. Swag: Splatting in the wild images with appearance-conditioned gaussians. In *European Conference on Computer Vision*, pages 325–340. Springer, 2024. 6, 15
- [4] Xiaobiao Du, Yida Wang, and Xin Yu. Mvgs: Multi-view-regulated gaussian splatting for novel view synthesis. *arXiv preprint arXiv:2410.02103*, 2024. 5
- [5] Yuheng Jiang, Zhehao Shen, Yu Hong, Chengcheng Guo, Yize Wu, Yingliang Zhang, Jingyi Yu, and Lan Xu. Robust dual gaussian splatting for immersive human-centric volumetric videos. *ACM Transactions on Graphics (TOG)*, 43(6):1–15, 2024. 1
- [6] Ying Jiang, Chang Yu, Tianyi Xie, Xuan Li, Yutao Feng, Huamin Wang, Minchen Li, Henry Lau, Feng Gao, Yin Yang, et al. Vr-gs: A physical dynamics-aware interactive gaussian splatting system in virtual reality. In *ACM SIGGRAPH 2024 Conference Papers*, pages 1–1, 2024. 1
- [7] Bernhard Kerbl, Georgios Kopanas, Thomas Leimkühler, and George Drettakis. 3d gaussian splatting for real-time radiance field rendering. *ACM Trans. Graph.*, 42(4):139–1, 2023. 1, 2, 3, 6, 7, 12, 15, 21
- [8] Diederik P Kingma. Adam: A method for stochastic optimization. *arXiv preprint arXiv:1412.6980*, 2014. 7
- [9] Jonas Kulhanek and Torsten Sattler. Nerfbaselines: Consistent and reproducible evaluation of novel view synthesis methods. *arXiv preprint arXiv:2406.17345*, 2024. 7
- [10] Jonas Kulhanek, Songyou Peng, Zuzana Kukelova, Marc Pollefeys, and Torsten Sattler. Wildgaussians: 3d gaussian splatting in the wild. *arXiv preprint arXiv:2407.08447*, 2024. 2, 3, 4, 6, 7, 11, 12, 13, 15
- [11] Peihao Li, Shaohui Wang, Chen Yang, Bingbing Liu, Weichao Qiu, and Haoqian Wang. Nerf-ms: Neural radiance fields with multi-sequence. In *Proceedings of the IEEE/CVF International Conference on Computer Vision*, pages 18591–18600, 2023. 2, 3, 4
- [12] Yiming Li, Zehong Wang, Yue Wang, Zhiding Yu, Zan Gojcic, Marco Pavone, Chen Feng, and Jose M Alvarez. Memorize what matters: Emergent scene decomposition from multitraverse. *arXiv preprint arXiv:2405.17187*, 2024. 1
- [13] Yiyi Liao, Jun Xie, and Andreas Geiger. Kitti-360: A novel dataset and benchmarks for urban scene understanding in 2d and 3d. *IEEE Transactions on Pattern Analysis and Machine Intelligence*, 45(3):3292–3310, 2022. 13
- [14] Jingyu Lin, Jiaqi Gu, Lubin Fan, Bojian Wu, Yujing Lou, Renjie Chen, Ligang Liu, and Jieping Ye. Hybrids: Decoupling transients and statics with 2d and 3d gaussian splatting. *arXiv preprint arXiv:2412.03844*, 2024. 2, 4, 6, 7, 11, 12, 13, 15
- [15] Minghua Liu, Ruoxi Shi, Linghao Chen, Zhuoyang Zhang, Chao Xu, Xinyue Wei, Hansheng Chen, Chong Zeng, Jiayuan Gu, and Hao Su. One-2-3-45++: Fast single image to 3d objects with consistent multi-view generation and 3d diffusion. In *Proceedings of the IEEE/CVF Conference on Computer Vision and Pattern Recognition*, pages 10072–10083, 2024. 1
- [16] Saswat Subhajyoti Mallick, Rahul Goel, Bernhard Kerbl, Markus Steinberger, Francisco Vicente Carrasco, and Fernando De La Torre. Taming 3dgs: High-quality radiance fields with limited resources. In *SIGGRAPH Asia 2024 Conference Papers*, pages 1–11, 2024. 3
- [17] Ricardo Martin-Brualla, Noha Radwan, Mehdi SM Sajjadi, Jonathan T Barron, Alexey Dosovitskiy, and Daniel Duckworth. Nerf in the wild: Neural radiance fields for unconstrained photo collections. In *Proceedings of the IEEE/CVF conference on computer vision and pattern recognition*, pages 7210–7219, 2021. 2, 3, 4, 6, 15
- [18] Ben Mildenhall, Pratul P Srinivasan, Matthew Tancik, Jonathan T Barron, Ravi Ramamoorthi, and Ren Ng. Nerf: Representing scenes as neural radiance fields for view synthesis. *Communications of the ACM*, 65(1):99–106, 2021. 1, 2, 3, 6, 15
- [19] Thang-Anh-Quan Nguyen, Luis Roldão, Nathan Piasco, Moussab Bennehar, and Dzmitry Tsishkou. Rodus: Robust decomposition of static and dynamic elements in urban scenes. In *European Conference on Computer Vision*, pages 112–130. Springer, 2024. 2
- [20] Maxime Oquab, Timothée Darcet, Théo Moutakanni, Huy Vo, Marc Szafraniec, Vasil Khalidov, Pierre Fernandez, Daniel Haziza, Francisco Massa, Alaaeldin El-Nouby, et al. Dinov2: Learning robust visual features without supervision. *arXiv preprint arXiv:2304.07193*, 2023. 2, 3, 7
- [21] Julian Ost, Fahim Mannan, Nils Thuerey, Julian Knodt, and Felix Heide. Neural scene graphs for dynamic scenes. In *Proceedings of the IEEE/CVF Conference on Computer Vision and Pattern Recognition*, pages 2856–2865, 2021. 2
- [22] Weining Ren, Zihan Zhu, Boyang Sun, Jiaqi Chen, Marc Pollefeys, and Songyou Peng. Nerf on-the-go: Exploiting uncertainty for distractor-free nerfs in the wild. In *Proceedings of the IEEE/CVF Conference on Computer Vision and Pattern Recognition*, pages 8931–8940, 2024. 6, 7, 11, 12, 13, 15

- [23] Sara Sabour, Suhani Vora, Daniel Duckworth, Ivan Krasin, David J Fleet, and Andrea Tagliasacchi. Robustnerf: Ignoring distractors with robust losses. In *Proceedings of the IEEE/CVF Conference on Computer Vision and Pattern Recognition*, pages 20626–20636, 2023. 4, 6, 7, 15
- [24] Sara Sabour, Lily Goli, George Kopanas, Mark Matthews, Dmitry Lagun, Leonidas Guibas, Alec Jacobson, David J Fleet, and Andrea Tagliasacchi. Spotlessplats: Ignoring distractors in 3d gaussian splatting. *arXiv preprint arXiv:2406.20055*, 2024. 2, 4, 6, 7, 15
- [25] Johannes Lutz Schönberger, Enliang Zheng, Marc Pollefeys, and Jan-Michael Frahm. Pixelwise View Selection for Unstructured Multi-View Stereo. In *European Conference on Computer Vision (ECCV)*, 2016. 4
- [26] Seungjoo Shin, Jaesik Park, and Sunghyun Cho. Locality-aware gaussian compression for fast and high-quality rendering. *arXiv preprint arXiv:2501.05757*, 2025. 2
- [27] Noah Snavely, Steven M Seitz, and Richard Szeliski. Photo tourism: exploring photo collections in 3d. In *ACM siggraph 2006 papers*, pages 835–846. ACM, 2006. 6, 11, 12, 13
- [28] Yuzhou Tang, Dejun Xu, Yongjie Hou, Zhenzhong Wang, and Min Jiang. Nexussplats: Efficient 3d gaussian splatting in the wild. *arXiv preprint arXiv:2411.14514*, 2024. 6, 15
- [29] Haithem Turki, Jason Y Zhang, Francesco Ferroni, and Deva Ramanan. Suds: Scalable urban dynamic scenes. In *Proceedings of the IEEE/CVF Conference on Computer Vision and Pattern Recognition*, pages 12375–12385, 2023. 2
- [30] Michael Van den Bergh, Xavier Boix, Gemma Roig, and Luc Van Gool. Seeds: Superpixels extracted via energy-driven sampling. *International Journal of Computer Vision*, 111: 298–314, 2015. 4
- [31] Peng Wang, Yuan Liu, Zhaoxi Chen, Lingjie Liu, Ziwei Liu, Taku Komura, Christian Theobalt, and Wenping Wang. F2-nerf: Fast neural radiance field training with free camera trajectories. In *Proceedings of the IEEE/CVF Conference on Computer Vision and Pattern Recognition*, pages 4150–4159, 2023. 2
- [32] Shuaixian Wang, Haoran Xu, Yaokun Li, Jiwei Chen, and Guang Tan. Ie-nerf: Inpainting enhanced neural radiance fields in the wild. *arXiv preprint arXiv:2407.10695*, 2024. 6, 15
- [33] Yihao Wang, Marcus Klasson, Matias Turkulainen, Shuzhe Wang, Juho Kannala, and Arno Solin. Desplat: Decomposed gaussian splatting for distractor-free rendering. *arXiv preprint arXiv:2411.19756*, 2024. 2, 4, 6, 7, 8, 11, 15
- [34] Zhou Wang, Alan C Bovik, Hamid R Sheikh, and Eero P Simoncelli. Image quality assessment: from error visibility to structural similarity. 13(4):600–612, 2004. 6
- [35] Guanjun Wu, Taoran Yi, Jiemin Fang, Lingxi Xie, Xiaopeng Zhang, Wei Wei, Wenyu Liu, Qi Tian, and Xinggang Wang. 4d gaussian splatting for real-time dynamic scene rendering. In *Proceedings of the IEEE/CVF Conference on Computer Vision and Pattern Recognition*, pages 20310–20320, 2024. 2
- [36] Hongchi Xia, Zhi-Hao Lin, Wei-Chiu Ma, and Shenlong Wang. Video2game: Real-time interactive realistic and browser-compatible environment from a single video. In *Proceedings of the IEEE/CVF Conference on Computer Vision and Pattern Recognition*, pages 4578–4588, 2024. 1
- [37] Jiachong Xu, Yiqun Mei, and Vishal M Patel. Wild-gs: Real-time novel view synthesis from unconstrained photo collections. *arXiv preprint arXiv:2406.10373*, 2024. 2, 3, 6, 7, 15
- [38] Jiawei Yang, Boris Ivanovic, Or Litany, Xinshuo Weng, Seung Wook Kim, Boyi Li, Tong Che, Danfei Xu, Sanja Fidler, Marco Pavone, et al. Emernerf: Emergent spatial-temporal scene decomposition via self-supervision. *arXiv preprint arXiv:2311.02077*, 2023. 2
- [39] Lihe Yang, Bingyi Kang, Zilong Huang, Xiaogang Xu, Jiashi Feng, and Hengshuang Zhao. Depth anything: Unleashing the power of large-scale unlabeled data. In *Proceedings of the IEEE/CVF Conference on Computer Vision and Pattern Recognition*, pages 10371–10381, 2024. 2, 3, 7
- [40] Yifan Yang, Shuhai Zhang, Zixiong Huang, Yubing Zhang, and Mingkui Tan. Cross-ray neural radiance fields for novel-view synthesis from unconstrained image collections. In *Proceedings of the IEEE/CVF International Conference on Computer Vision*, pages 15901–15911, 2023. 2, 3, 4, 6, 7, 8, 15
- [41] Ziyi Yang, Xinyu Gao, Wen Zhou, Shaohui Jiao, Yuqing Zhang, and Xiaogang Jin. Deformable 3d gaussians for high-fidelity monocular dynamic scene reconstruction. In *Proceedings of the IEEE/CVF Conference on Computer Vision and Pattern Recognition*, pages 20331–20341, 2024. 4, 11
- [42] Zehao Yu, Anpei Chen, Binbin Huang, Torsten Sattler, and Andreas Geiger. Mip-splatting: Alias-free 3d gaussian splatting. In *Proceedings of the IEEE/CVF Conference on Computer Vision and Pattern Recognition*, pages 19447–19456, 2024. 6, 15
- [43] Zehao Yu, Torsten Sattler, and Andreas Geiger. Gaussian opacity fields: Efficient and compact surface reconstruction in unbounded scenes. *arXiv preprint arXiv:2404.10772*, 2024. 6, 15
- [44] Dongbin Zhang, Chuming Wang, Weitao Wang, Peihao Li, Minghan Qin, and Haoqian Wang. Gaussian in the wild: 3d gaussian splatting for unconstrained image collections. In *European Conference on Computer Vision*, pages 341–359. Springer, 2024. 4, 6, 7, 8, 12, 13, 15
- [45] Richard Zhang, Phillip Isola, Alexei A Efros, Eli Shechtman, and Oliver Wang. The unreasonable effectiveness of deep features as a perceptual metric. In *Proceedings of the IEEE conference on computer vision and pattern recognition*, pages 586–595, 2018. 6
- [46] Zheng Zhang, Wenbo Hu, Yixing Lao, Tong He, and Hengshuang Zhao. Pixel-gs: Density control with pixel-aware gradient for 3d gaussian splatting. In *European Conference on Computer Vision*, pages 326–342. Springer, 2024. 3, 5, 7
- [47] Xiaoyu Zhou, Zhiwei Lin, Xiaojun Shan, Yongtao Wang, Deqing Sun, and Ming-Hsuan Yang. Drivinggaussian: Composite gaussian splatting for surrounding dynamic autonomous driving scenes. In *Proceedings of the IEEE/CVF Conference on Computer Vision and Pattern Recognition*, pages 21634–21643, 2024. 1

ForestSplats: Deformable transient field for Gaussian Splatting in the Wild

Supplementary Material

In this supplementary materials, we provide a detailed description of the more complete experimental settings, along with additional qualitative and quantitative results, including metrics that were not included in the main paper due to the page limitations. Furthermore, we present additional ablation studies, detailed analyses and observations, and provide failure cases. We also discuss potential future directions. The contents are summarized as follows:

- Sec. 9: More implementation details
- Sec. 10: More experimental results
- Sec. 11: More ablation studies
- Sec. 12: User study
- Sec. 13: Failure cases and Future works

9. More Implementation details

9.1. Architecture

Our method is based on the WildGaussians [10] codebase. For the deformable transient field, we follow Deform3D-GS [41] for modeling transient elements. We train a deformable MLP f_d with the transient field to capture transient elements. Otherwise, we design a color mapping MLP f_c consisting of eight fully connected layers with ReLU activations, 256-dimensional hidden layers, and a 256-dimensional output. We use transient embedding per image $t \in \mathbb{R}^{32}$ for deformable MLP f_d . During inference phase, we only leverage static field for novel-view synthesis.

9.2. Photo Tourism & NeRF On-the-go

For the Photo Tourism dataset [27], we optimize for 200K iterations to train a representation of the entire scene. For the NeRF On-the-go dataset [22], we optimize for 30K iterations. Most hyperparameter settings follow the default codebase [10]. To represent transient elements and handle appearance changes in the Photo Tourism dataset [27], we leverage an appearance MLP, following WildGaussians [10]. Additionally, we introduce a multi-stage training scheme, where \mathcal{L}_{init} is applied up to 80K iterations, followed by \mathcal{L}_{mid} until 120K iterations, and finally, \mathcal{L}_{total} is used for the remaining steps. For the NeRF On-the-go dataset [22], we apply \mathcal{L}_{init} for the first 15K iterations, continue with \mathcal{L}_{mid} until 20K iterations, and finally switch to \mathcal{L}_{total} .

10. More experimental results

We provided additional experiment results to demonstrate a more comprehensive evaluation of our methods on the Photo Tourism [27] and NeRF On-the-go [22] datasets. Fur-

Scene	Method	Memory	Scene	Method	Memory
Mountain	Desplat [33]	29.03	Fountain	Desplat [33]	37.81
	HybridGS [14]	44.29		HybridGS [14]	57.68
	ForestSplats (Ours)	2.28		ForestSplats (Ours)	2.29
Patio	Desplat [33]	22.28	Spot	Desplat [33]	41.86
	HybridGS [14]	33.99		HybridGS [14]	63.86
	ForestSplats (Ours)	2.26		ForestSplats (Ours)	2.27

Table 6. Comparison of memory usage efficiency. We report CPU Memory usage (MB) for the initial number of transient Gaussians.

thermore, we provide additional qualitative results to validate the effectiveness of each component in Fig. 24. Moreover, we highly recommend that the reader watch the several videos on the [webpage](#). Our method achieves consistency and high-quality novel-view synthesis.

10.1. More Photo Tourism results

As illustrated in Fig. 18 and Tab. 9, our methods achieve high-quality rendering and show competitive performance compared to existing methods without VFM. Wild-GS and WildGaussians use semantic features from pre-trained VFM to generalize static scenes. In contrast, our method effectively decomposes transient elements from static scenes without VFM. Furthermore, we gradually interpolate between two appearance embeddings, as shown in Fig. 20. The results indicate the smoothness and consistency of the appearance embedding.

10.2. More NeRF On-the-go results

For NeRF On-the-go dataset [22], we visualize additional results of the remaining scenes due to page limitations as shown in Fig. 19. NeRF On-the-go [22] and WildGaussians [10] tackle transient elements using semantic features from the Vision Foundation model. However, our method addresses transient elements by considering photometric errors and superpixels. The detailed quantitative results demonstrate that ForestSplats outperforms the prior methods in Tab. 10. Specifically, our ForestSplats achieves state-of-the-art performance across five scenes, showing high-quality results.

11. More ablation studies

11.1. Efficiency of deformable transient field

As shown in Tab. 6 and Tab. 7, we emphasize the advantages of our method, particularly in terms of memory usage and efficiency. Although ForestSplats requires the Deformable MLP and the color mapping MLP, our method efficiently

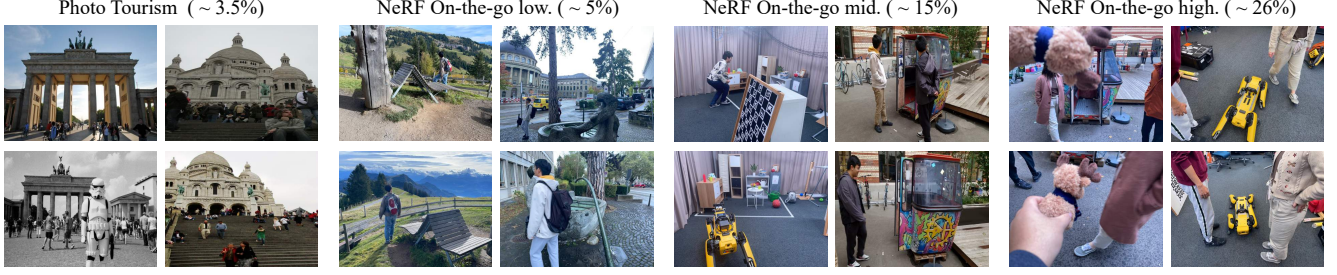


Figure 13. Visualization of sample training images. We present occluders in the Photo Tourism and NeRF On-the-go datasets.

Scene	Method	Memory usage (MB)		Testing FPS
		Static field	Transient field	
Corner	3D-GS [7]	410.70	0	116
	HybridGS [14]	42.20	34.70	160
	ForestSplats (Ours)	58.0	2.27	143
Trevi	GS-W [10]	91.21	0	38
Fountain	ForestSplats (Ours)	30.5	3.39	103

Table 7. Comparison of memory usage (MB) and testing FPS.

Segments	PSNR \uparrow	SSIM \uparrow	LPIPS \downarrow
10	19.83	0.65	0.324
15	21.47	0.711	0.198
20	22.61	0.781	0.145
25	22.21	0.738	0.199

Table 8. Comparison of the number of superpixels.

utilizes memory to represent transient elements. Compared to GS-W [44], our method demonstrates remarkable computational efficiency on the Trevi Fountain scene in Tab. 7.

11.2. Effectiveness of superpixel-aware mask

As shown in Fig. 21, superpixel-aware mask effectively captures the transient elements compared to the existing methods. Furthermore, we demonstrate that our method explicitly decomposes the transient elements from the 2D scenes, as provided in Fig. 22. Moreover, we provide additional results for the multi-stage training scheme in Fig. 14. We also provide detailed results for the number of superpixels in Tab. 8. As shown in Fig. 13, the distribution of transient elements varies between the Photo Tourism and NeRF On-the-go datasets. Therefore, adjusting the number of superpixels for each scene could enhance performance.

11.3. Proof of positional gradient

We provide a step-by-step proof that the positional gradient is generally directed towards a region of static elements. The gradient is calculated by:

$$\mathcal{G}_{i,x} = \frac{\partial \mathcal{L}}{\partial \mu_{i,x}} = \sum_{k=1}^p \frac{\partial \mathcal{L}_k}{\partial \mu_{i,x}}, \quad (11)$$

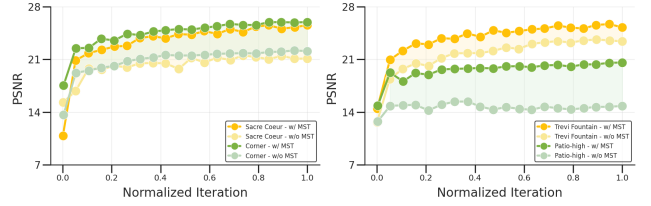


Figure 14. Comparison of training PSNR across with and without a multi-stage training scheme. MST denotes multi-stage training.

where \mathcal{L} denotes the rendering loss from \mathcal{L}_{GS} , p is the number of pixels covered by Gaussian \mathcal{G}_i , and $\mu_{i,x}$ is the pixel-space projection of Gaussian \mathcal{G}_i under viewpoint x . The computation for static Gaussians is as follows:

$$\frac{\partial \mathcal{L}_k^{(static)}}{\partial \mu_{i,x}} \propto (1 - \mathcal{M}_S(x_k)) \frac{\partial \mathcal{L}_k}{\partial \mu_{i,x}}. \quad (12)$$

On the other hand, the positional gradient for transient Gaussians is computed as:

$$\frac{\partial \mathcal{L}_k^{(transient)}}{\partial \mu_{i,x}} \propto \mathcal{M}_S(x_k) \frac{\partial \mathcal{L}_k}{\partial \mu_{i,x}}. \quad (13)$$

Thus, the positional gradient is influenced by the superpixel-aware mask \mathcal{M}_S . In the Photo Tourism [27] and NeRF On-the-Go datasets [22], transient elements typically constitute less than 30%. Consequently, the gradient tends to be directed toward regions of static elements.

11.4. Discussion of uncertainty-aware densification

We further demonstrate that our uncertainty-aware densification (UAD) effectively removes high-uncertainty static Gaussians, thereby enhancing the consistency and reconstruction quality in Fig. 15 and Fig. 23. Specifically, UAD enhances depth consistency compared to the case without UAD, as illustrated in Fig. 15. Furthermore, we performed an additional evaluation using SIFT-based feature matching on images rendered with and without UAD. As shown in Fig. 23, leveraging UAD ensures that feature correspondences remain consistent across different viewpoints by removing high-uncertainty static Gaussians and avoiding generating static Gaussian in the region of transient elements.

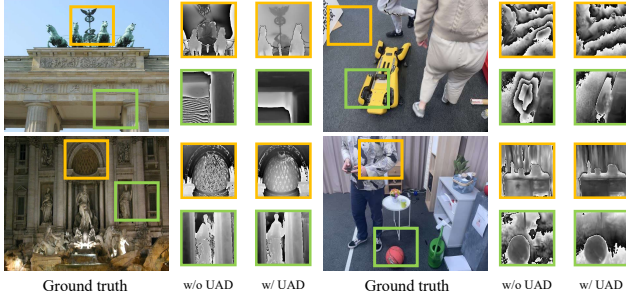


Figure 15. Comparison of depth consistency w/o and w/ UAD.

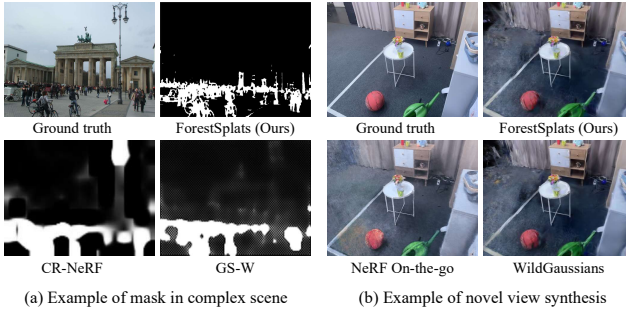


Figure 16. Failure cases of our method. (a) Our method fails to capture fine details in masks within complex scenes. (b) Furthermore, our method fails to generalize to sparse training views.

12. User study

12.1. User evaluation results

We recruited several researchers as survey participants and asked them to complete a questionnaire, as shown in Fig. 25. The questionnaire includes several questions and rendering results comparing our method with baselines on three different scenes. Baseline methods include WildGaussians [10], GS-W [44], NeRF On-the-go [22]. Each participant was asked to evaluate the rendering videos on a scale from 1 (poor) to 5 (excellent). The average scores for each question are visualized in Fig. 17. The results show that our method achieved the highest scores across all aspects, including transient removal, floater reduction, and consistency quality, demonstrating the effectiveness of our approach.

13. Failure cases and Future works

13.1. Failure cases

Our method shows impressive results in capturing transient elements. However, similar to prior methods, our method struggles to accurately mask transient elements, as shown in Fig. 16-(a) due to complex real-world environments. Furthermore, as shown in Fig. 16-(b), our method often fails to generalize in novel-view synthesis, especially in scenarios

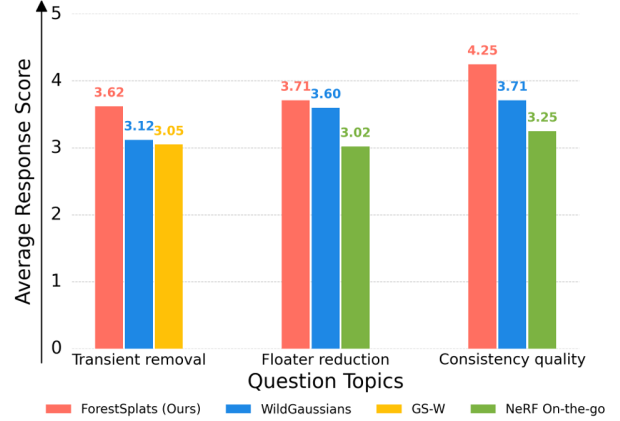


Figure 17. User Study Results: Average response scores on transient removal, floater reduction, and consistency quality.

with sparse training views.

13.2. Future works

Our method explicitly decomposes a complex scene into static and transient fields. However, transient elements are ephemeral and short-lived in the scenes. As a result, the absence of multi-view consistency eliminates the need to consider depth. Thus, deforming the 2D transient field of HybridGS [14], which consists of Gaussians with nine parameters, improves efficiency and reduces memory usage. Specifically, while we demonstrate the effectiveness of our methods on the Photo Tourism [27] and NeRF On-the-Go [22] datasets, another promising direction is extending our approach to large-scale dynamic scenes such as KITTI-360 [13] and NuScenes [1]. We leave this as future work.



Figure 18. Additional qualitative results from novel-view synthesis on the Photo Tourism dataset.

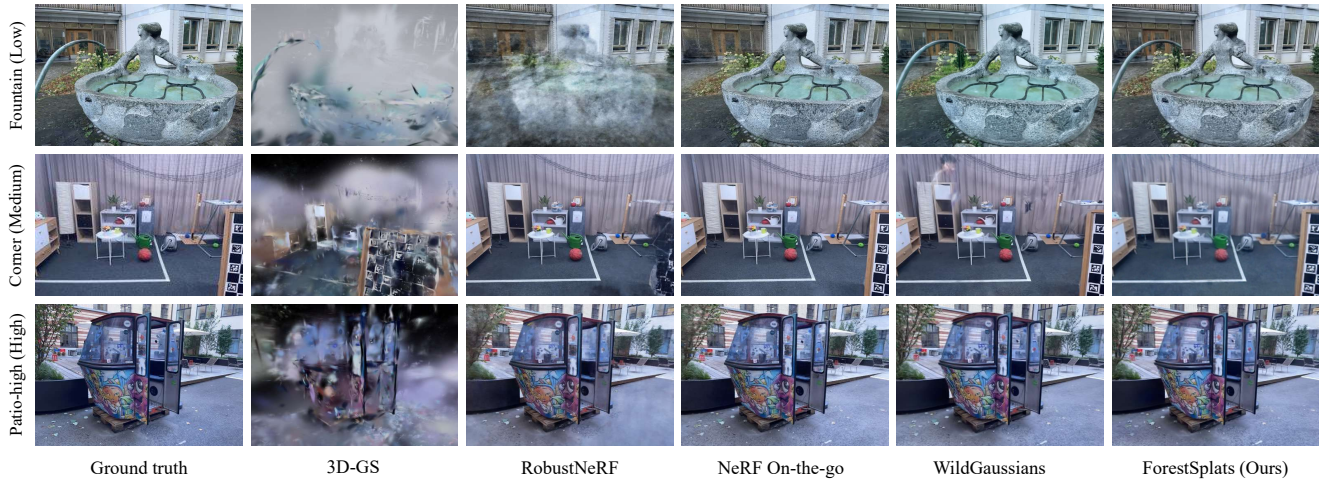


Figure 19. Additional qualitative results from novel-view synthesis on the NeRF On-the-go dataset.

Method	Brandenburg Gate			Sacre Coeur			Trevi Fountain		
	PSNR↑	SSIM↑	LPIPS↓	PSNR↑	SSIM↑	LPIPS↓	PSNR↑	SSIM↑	LPIPS↓
3D-GS [7]	19.33	0.884	0.132	17.70	0.845	0.176	17.08	0.714	0.241
NeRF-W [17]	24.17	0.891	0.167	19.20	0.808	0.192	18.97	0.698	0.265
Ha-NeRF [18]	24.04	0.887	0.139	20.02	0.801	0.171	20.18	0.691	0.223
DeSplat [33]	25.04	0.92	0.142	20.14	0.868	0.178	23.31	0.775	0.226
CR-NeRF [40]	26.53	0.900	0.106	22.07	0.823	0.152	21.48	0.712	0.207
RobustNeRF [23]	25.79	0.923	<u>0.094</u>	20.94	0.852	0.137	23.58	0.785	0.170
IE-NeRF [32]	25.33	0.898	0.158	20.37	0.861	0.169	20.76	0.719	0.217
SWAG [3]	26.33	0.929	0.139	21.16	0.86	0.185	23.10	0.815	0.208
WildGaussian [10]	27.77	0.927	0.133	22.56	0.859	0.177	23.63	0.766	0.228
NexusSplats [28]	27.76	0.922	0.141	23.13	0.859	0.174	23.96	0.766	0.240
GS-W [44]	27.96	0.932	0.086	23.24	0.863	0.130	22.91	0.801	0.156
Wild-GS [37]	29.65	<u>0.933</u>	0.095	24.99	0.878	<u>0.127</u>	24.45	<u>0.808</u>	<u>0.162</u>
ForestSplats (Ours)	<u>28.13</u>	0.935	0.118	<u>23.84</u>	<u>0.876</u>	0.123	<u>24.11</u>	0.802	0.213

Table 9. Quantitative results on Photo Tourism dataset. The bold and underlined numbers indicate the best and second-best results.

Method	Low Occlusion						Medium Occlusion						High Occlusion					
	Mountain			Fountain			Corner			Patio			Spot			Patio-High		
	PSNR↑	SSIM↑	LPIPS↓	PSNR↑	SSIM↑	LPIPS↓	PSNR↑	SSIM↑	LPIPS↓	PSNR↑	SSIM↑	LPIPS↓	PSNR↑	SSIM↑	LPIPS↓	PSNR↑	SSIM↑	LPIPS↓
RobustNeRF [23]	17.54	0.496	0.383	15.65	0.318	0.576	23.04	0.764	0.244	20.39	0.718	0.251	20.65	0.625	0.391	20.54	0.578	0.366
Gaussian Opacity Field [43]	19.86	0.649	0.200	20.19	0.672	0.189	21.15	0.728	0.230	18.31	0.639	0.328	20.18	0.689	0.338	18.31	0.639	0.328
3D-GS [7]	19.40	0.638	0.213	19.96	0.659	<u>0.185</u>	20.90	0.713	0.241	17.48	0.704	0.199	20.77	0.693	0.316	17.29	0.604	0.363
Mip-Splatting [42]	20.70	0.661	0.169	20.37	0.662	0.187	21.53	0.739	0.241	15.58	0.491	0.536	20.03	0.683	0.324	15.58	0.491	0.536
GS-W [44]	19.43	0.596	0.299	20.06	<u>0.723</u>	0.274	22.17	0.793	0.155	19.90	0.681	0.260	17.13	0.608	0.409	19.90	0.681	0.260
NeRF On-the-go [22]	20.46	0.661	0.186	20.79	0.661	0.195	23.74	0.806	0.127	20.88	0.754	0.133	22.80	0.800	0.132	21.57	0.706	0.205
WildGaussians [10]	20.43	0.653	0.255	20.81	0.662	0.215	24.16	0.822	0.045	21.44	0.800	0.138	23.82	0.816	0.138	22.23	0.725	0.206
SpotLessSplats* [24]	19.84	0.58	0.294	20.19	0.612	0.258	24.03	0.795	0.258	21.55	<u>0.838</u>	<u>0.065</u>	23.52	0.756	0.185	20.31	0.664	0.259
DeSplat [33]	19.59	<u>0.710</u>	<u>0.170</u>	20.27	0.680	0.170	<u>26.05</u>	<u>0.880</u>	<u>0.090</u>	20.89	0.810	0.110	26.07	0.900	0.090	<u>22.59</u>	0.840	0.120
HybridGS [14]	<u>21.73</u>	0.693	0.284	<u>21.11</u>	0.674	0.252	25.03	0.847	0.151	21.98	0.812	0.169	24.33	0.794	0.196	21.77	0.741	0.211
ForestSplats (Ours)	22.17	0.736	0.235	21.62	0.741	0.198	26.17	0.891	0.136	<u>21.76</u>	0.849	0.134	<u>25.94</u>	<u>0.846</u>	<u>0.109</u>	22.74	<u>0.784</u>	<u>0.129</u>

Table 10. Quantitative results on NeRF On-the-go dataset. The bold and underlined numbers indicate the best and second-best results. * indicates that the results are reproduced from the official code.



Figure 20. Visualization of appearance interpolation. We gradually interpolate from the source appearance to the target appearance.



Figure 21. Comparison of transient mask quality with existing methods on the Photo Tourism dataset.

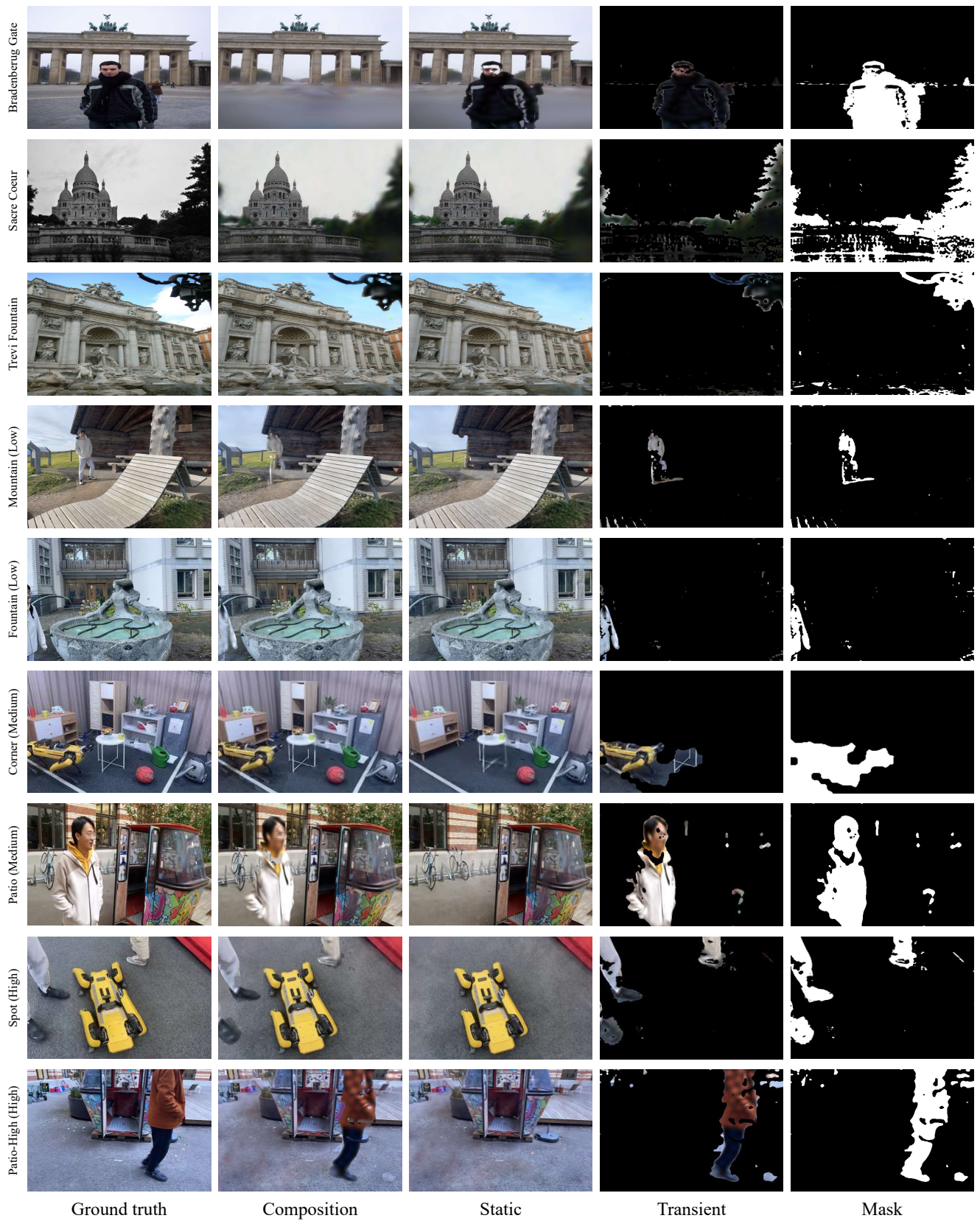


Figure 22. Additional novel-view synthesis results for static and transient elements on the Photo Tourism and NeRF On-the-go datasets.

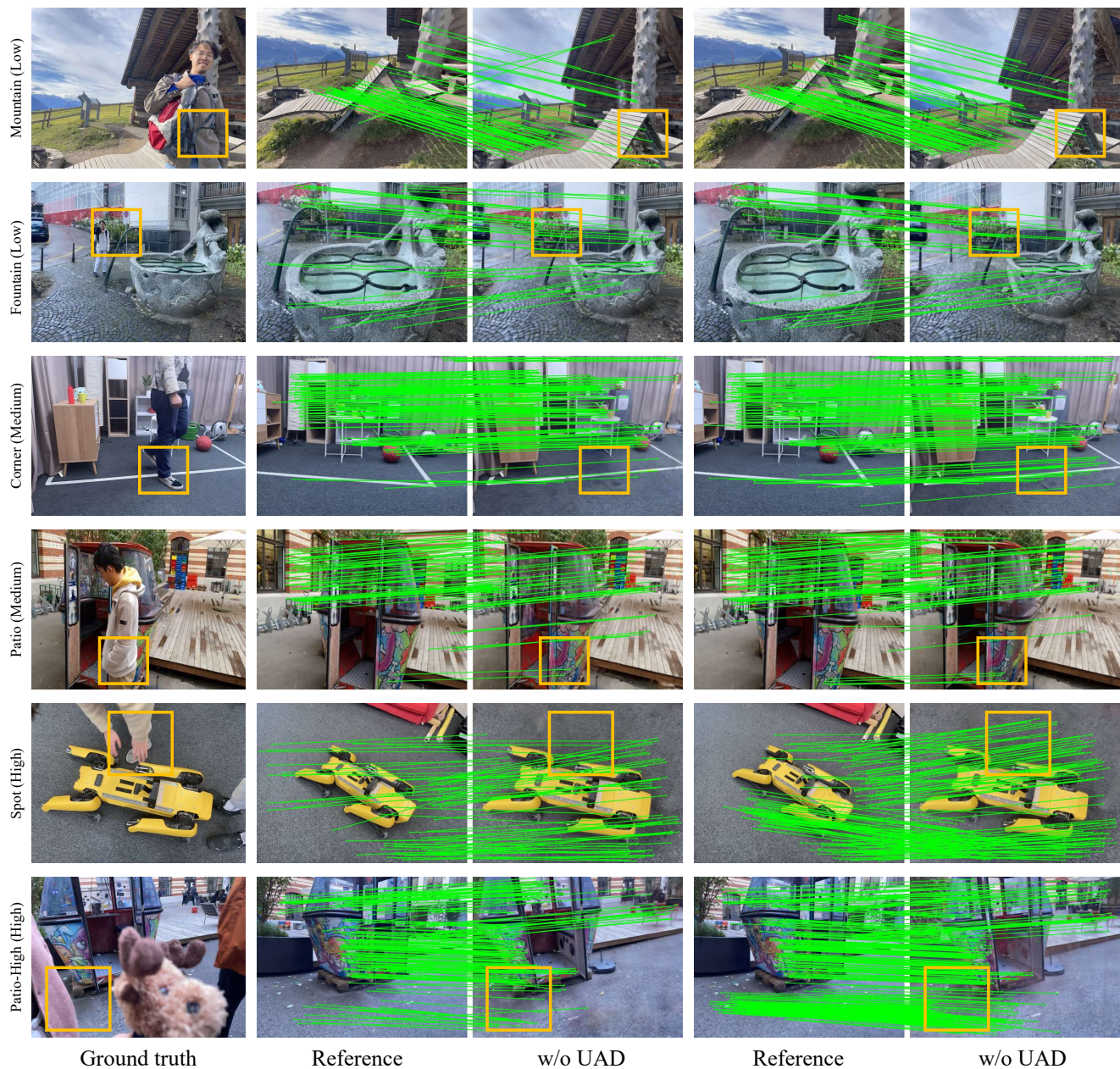


Figure 23. Comparison of image matching results on the NeRF On-the-go dataset with and without UAD across all scenes.

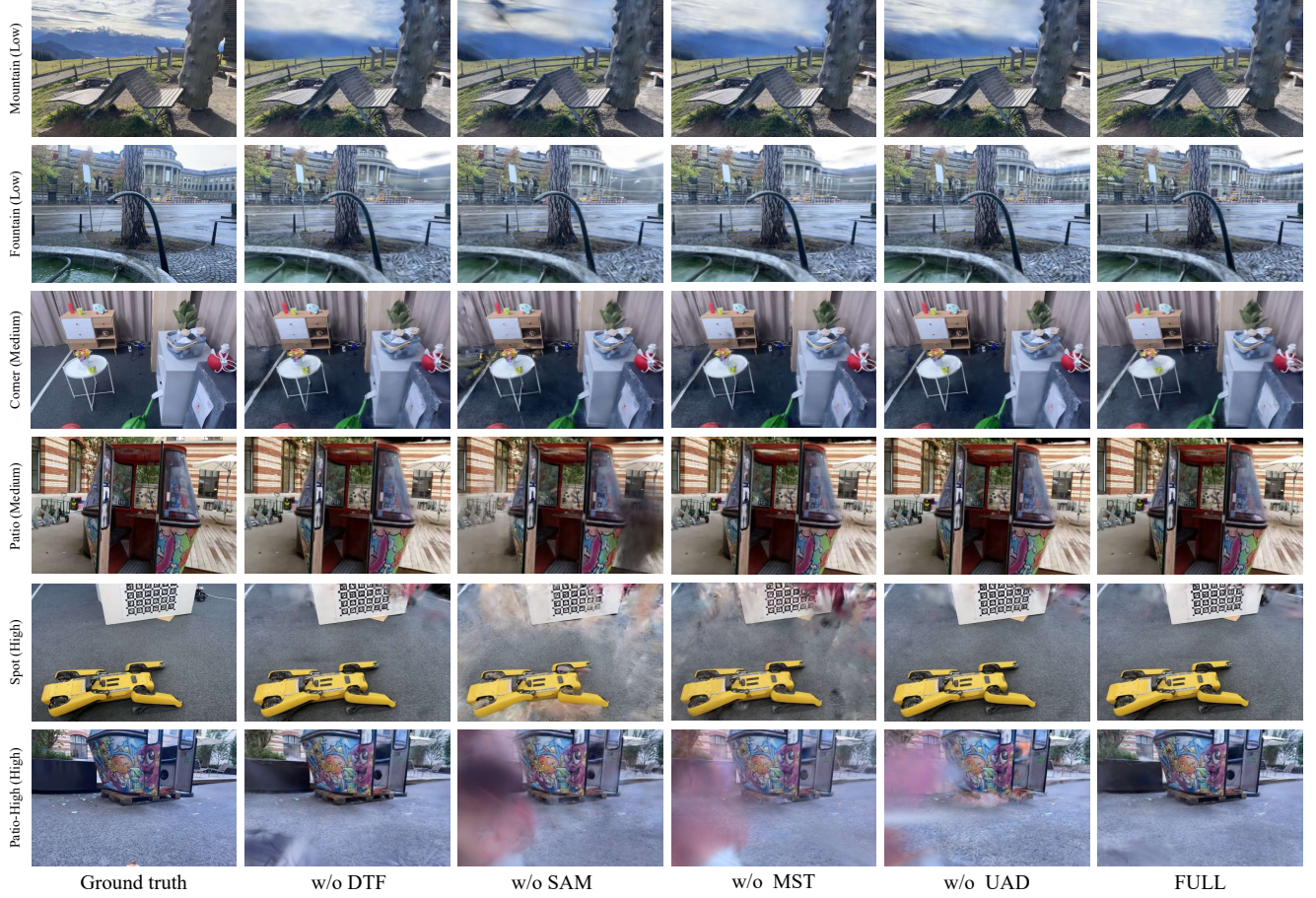


Figure 24. More qualitative results for each component in ForestSplats. DTF, SAM, MST, and UAD denote Deformable MLP, Superpixel-aware mask, Multi-stage training scheme, and Uncertainty-aware densification.

1. Trevi Fountain (Photo Tourism dataset)



(a)



(b)



(c)

2. Patio-high (NeRF On-the-go dataset)



(a)



(b)



(c)

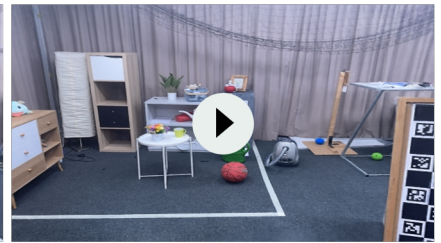
3. Corner (NeRF On-the-go dataset)



(a)



(b)



(c)

Question 1. How naturally do you think the transient distractors were removed?

Question 2. How naturally does the scene appear without the interference of the floaters?

Question 3. How well do the rendering results consistently maintain quality?

Figure 25. Our user study questionnaire. Each participant was shown an upper figure, which is a rendering video of several scenes using different methods. After watching the video, they were asked to answer the question below.

Notation	Shape	Definition
μ	\mathbb{R}^3	Position of Gaussians in 3DGS [7]
Σ	$\mathbb{R}^{3 \times 3}$	Covariance matrix of Gaussians
α	\mathbb{R}^1	Opacity of Gaussians
c	\mathbb{R}^3	View-dependent color of Gaussians
W	$\mathbb{R}^{3 \times 3}$	Viewing transformation matrix
J	$\mathbb{R}^{2 \times 3}$	Jacobian of the affine approximation of the projective transformation
K		Number of Gaussians contributed to the rendering
C	\mathbb{R}^3	The obtained pixel value after rendering
M	\mathbb{R}^1	Transient element mask
\hat{I}	$\mathbb{R}^{3 \times H \times W}$	Rendered image
I_{gt}	$\mathbb{R}^{3 \times H \times W}$	Ground truth image
\hat{I}_d	$\mathbb{R}^{3 \times H \times W}$	Rendered image with transient elements
\hat{I}_s	$\mathbb{R}^{3 \times H \times W}$	Rendered image with static elements
t_i	\mathbb{R}^{32}	Transient embedding per image i
$\Delta\mu$	\mathbb{R}^3	Offset for the Gaussian's position
Δs	\mathbb{R}^3	Offset for the Gaussian's scaling
Δr	\mathbb{R}^4	Offset for the Gaussian's rotation
ρ	\mathbb{R}	Mask coverage ratio for each superpixel s
\mathcal{M}_O		Transient element mask from Unet S_θ
S_θ		Learnable CNN to mask transient elements
\mathcal{S}		The set where I_{gt} is partitioned into superpixels
s		The elements of \mathcal{S}
\mathcal{M}_S		Superpixel-aware mask
$l^{(u)}$	\mathbb{R}^n	Uncertainty parameter for static Gaussians
\mathbf{g}		View-space positional gradient
\mathcal{L}_{GS}		The loss item used in 3DGS [7]
\mathcal{L}_{BCE}		The loss to mitigate the undesired blending of Gaussians between static and transient fields
\mathcal{L}_{init}		The loss to train the static field \mathcal{G}_s
\mathcal{L}_{mid}		The loss to train the Unet S_θ and transient field \mathcal{G}_d
λ		A weighting factor used in \mathcal{L}_{GS}
f_d		MLP predicting the attributes of transient Gaussians
f_c		MLP mapping the color of transient Gaussians
\mathcal{G}_s		Static field
\mathcal{G}_d		Deformable transient field

Table 11. For clarity and to avoid confusion in notation, we provided notation table.